


# Dissipative Preparation of Generalized Bell States with the Sørensen-Mølmer Setting

P.Z. Zhao<sup>1</sup>, Z. Jin<sup>2,\*</sup> and D.M. Tong<sup>1,†</sup>

<sup>1</sup>*Department of Physics, Shandong University, Jinan 250100, China*

<sup>2</sup>*College of Sciences, Northeastern University, Shenyang 110819, China*

 (Received 12 September 2021; revised 22 March 2022; accepted 3 June 2022; published 21 July 2022)

Quantum entanglement is an important resource in quantum information processing tasks, such as quantum cryptography, quantum teleportation, and quantum computation. The main obstacle to faithful and reliable preparation of entangled states is environment-induced decoherence. Dissipative transition of a general quantum state to an entangled steady state provides an effective strategy to protect entanglement from decoherence, where the decoherence converts into an essential resource. In this paper, we put forward a scheme to prepare generalized Bell states based on trapped ions, in which unitary dynamics and spontaneous emission are combined to drive an arbitrary quantum state in the ground-state space to a unique steady state. The scheme is realized by using the renowned Sørensen-Mølmer setting and is therefore compatible with current experimental technology. Moreover, the vibrational degree of freedom is decoupled from the unitary dynamics so that the scheme does not need to cool the collective vibrational mode to its ground state and thus it works for thermally excited states. Besides, our scheme is demonstrated to be insensitive to variations of some parameters with the aid of numerical simulation.

DOI: [10.1103/PhysRevApplied.18.014051](https://doi.org/10.1103/PhysRevApplied.18.014051)

## I. INTRODUCTION

Quantum entanglement is an important resource in quantum information processing tasks, such as quantum cryptography [1], quantum teleportation [2], and quantum computation [3]. The main obstacle to faithful and reliable preparation of entangled states is the decoherence caused by the interaction between the quantum system and its environment. Interestingly, open systems may have steady states, which remain stable during the evolution and thus are immune to the environment-induced decoherence. This motivates researchers to protect entanglement by preparing the entangled state as the steady state. In the strategy, the unitary dynamics are combined with the dissipation to drive a general quantum state to an entangled steady state and thus the decoherence is no longer undesirable but converts into an essential resource. Due to this merit, dissipative preparation of entangled steady states has attracted much attention.

The early scheme for dissipative preparation of a maximally entangled state is based on cavity quantum electrodynamics [4]. It combines unitary dynamics with cavity decay to drive a quantum state to an entangled steady state but spontaneous emission from excited states to ground states is still a destructive noise source. Further research

has shown that the spontaneous emission can be also taken as a useful resource of preparing entangled states and a number of schemes for dissipative preparation of entanglement have been proposed based on cavity decay and spontaneous emission [5–13]. Furthermore, dissipative preparation of entanglement has been generalized to high-dimensional entanglement [9,10], multipartite entanglement [14–18], and distant entanglement [19]. Besides the schemes with cavity quantum electrodynamics, schemes for dissipative preparation of entanglement have been also put forward based on trapped ions [20–22], superconducting [23], nitrogen-vacancy centers in diamond [24–26], and Rydberg atoms [27–37]. Encouragingly, dissipative preparation of entanglement has been experimentally demonstrated with trapped ions [38], superconducting [39,40], and nitrogen-vacancy centers in diamond [41].

The trapped ion, owing to its merits of both a long coherence time and the ability to perform high-fidelity quantum operations, is an appealing physical system for the implementation of quantum information processing tasks. The early schemes for trapped-ion-based dissipative preparation of entanglement have been realized by using cold ions [20,21,38]. In these schemes, the collective vibrational mode of trapped ions needs to be cooled to its ground state. Moreover, the vibrational degree of freedom is coupled to the internal degree of freedom, making the preparation sensitive to vibrational quantum numbers. Subsequently, standing-wave lasers have been utilized to

\*jinzhao@mail.neu.edu.cn

†tdm@sdu.edu.cn

prepare entanglement [22]. This scheme needs two vibrational modes to produce standing-wave-based interaction but the interaction has not been experimentally realized since its proposal [42]. Additionally, the realized states in the previous schemes are only the maximally entangled singlet state  $(|\uparrow\downarrow\rangle - |\downarrow\uparrow\rangle)/\sqrt{2}$ , where  $|\uparrow\rangle$  and  $|\downarrow\rangle$  are the qubit states.

In this paper, we propose a scheme for dissipative preparation of generalized Bell states with trapped ions. The four Bell states, including the previously realized maximally entangled singlet state, are the specific case of our generalized Bell states. Our scheme is performed by using bichromatic lasers with the renowned Sørensen-Mølmer setting [43,44], where only a single vibrational mode is utilized. Different from the previous schemes with cold trapped ions, the vibrational degrees of freedom in our scheme are decoupled from the unitary dynamics so that the vibrational mode does not need to be cooled to its ground state and thus the preparation works for thermally excited states. This allows our scheme to avoid some of the shortcomings of the schemes based on cold ions, such as the infidelity of quantum operations due to the heating and dephasing of the ion motion caused by voltage fluctuations in the electrodes [45–47]. More importantly, our scheme is compatible with the current experimental technology, since the Sørensen-Mølmer setting has been demonstrated in many experiments [47–51]. Besides, our scheme is demonstrated to be insensitive to variations of some parameters with the aid of numerical simulation.

## II. THE SCHEME

Consider two four-level ions trapped in a linear trap. The four levels correspond to two ground states,  $|0\rangle$  and  $|1\rangle$ , and two excited states,  $|e_0\rangle$  and  $|e_1\rangle$ , as shown in Fig. 1(a). The generalized Bell states that we aim to prepare are

$$|\Phi\rangle = \frac{1}{\sqrt{2}}(|00\rangle + e^{i\phi}|11\rangle), \quad |\Psi\rangle = \frac{1}{\sqrt{2}}(|01\rangle + e^{-i\phi}|10\rangle), \quad (1)$$

where  $\phi$  is a time-independent arbitrary phase. The four Bell states

$$|\Phi^\pm\rangle = \frac{1}{\sqrt{2}}(|00\rangle \pm |11\rangle), \quad |\Psi^\pm\rangle = \frac{1}{\sqrt{2}}(|01\rangle \pm |10\rangle), \quad (2)$$

are the specific case of the above generalized Bell states.

To prepare the generalized Bell states in Eq. (1), we use resonant microwave pulses to drive the transitions between ground states and use bichromatic lasers to drive the transitions between ground states and excited states.

To start with, we describe the unitary dynamics induced by the ion-microwave interaction. We use two resonant microwave pulses with Rabi frequencies  $\Omega \exp(i\pi)$  and  $\Omega \exp(i\phi)$  to drive the transitions  $|0\rangle \leftrightarrow |1\rangle$  of ions 1 and 2, respectively. In the rotating frame and with the rotating-wave approximation, the Hamiltonian describing

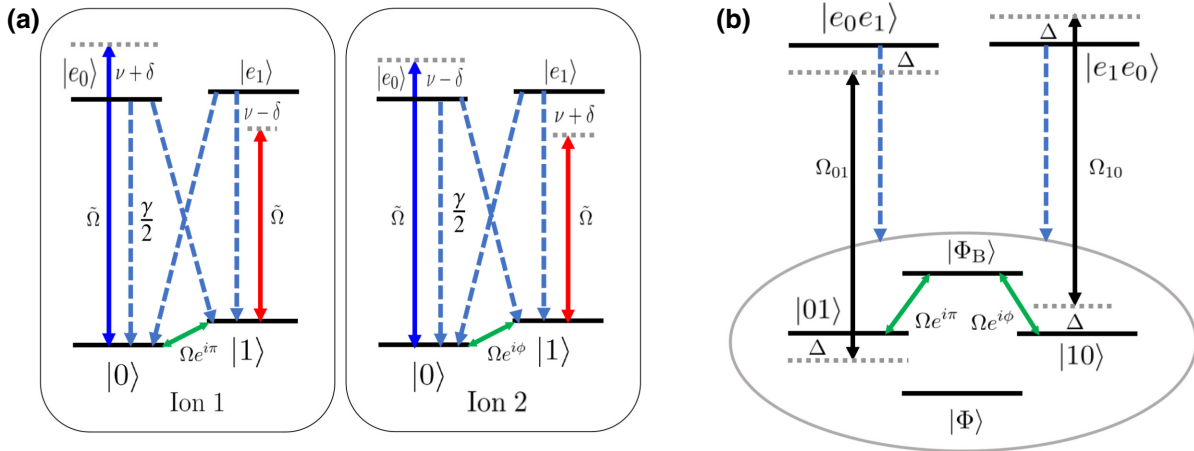


FIG. 1. The schematic setup for dissipative preparation of  $|\Phi\rangle$ . (a) The configuration of two four-level ions. The transitions  $|0\rangle \leftrightarrow |1\rangle$  of the two ions are driven by resonant microwave pulses. The transitions  $|0\rangle \leftrightarrow |e_0\rangle$  and  $|1\rangle \leftrightarrow |e_1\rangle$  of ion 1 are, respectively, driven by blue and red sideband lasers with detunings  $-(\nu + \delta)$  and  $\nu - \delta$  and the transitions  $|0\rangle \leftrightarrow |e_0\rangle$  and  $|1\rangle \leftrightarrow |e_1\rangle$  of ion 2 are, respectively, driven by blue and red sideband lasers with detunings  $-(\nu - \delta)$  and  $\nu + \delta$ . All the lasers share a common Rabi frequency  $\tilde{\Omega}$ . The spontaneous emission rate from the excited states  $|e_0\rangle$  and  $|e_1\rangle$  to the ground states  $|0\rangle$  and  $|1\rangle$  is  $\gamma/2$ . (b) The dynamical process combining unitary dynamics with dissipation. An arbitrary state in the ground-state space is directly or indirectly pumped to the excited-state subspace and then decays to the ground-state space. The state that decays to the ground-state space is to be repumped and will redecay until it turns into the unique steady state  $|\Phi\rangle$ .

ion-microwave interaction reads

$$H_m = \Omega e^{i\pi} |1\rangle_{11} \langle 0| + \Omega e^{i\phi} |1\rangle_{22} \langle 0| + \text{H.c.}, \quad (3)$$

where H.c. represents the Hermitian conjugate terms and  $|k\rangle_j$  represents the state  $|k\rangle$  of the  $j$ th ion. By using the double-ion-state representation, the above Hamiltonian can be rewritten as

$$H_m = \sqrt{2}\Omega |01\rangle \langle \Phi_B| - \sqrt{2}\Omega e^{i\phi} |\Phi_B\rangle \langle 10| + \text{H.c.} \quad (4)$$

in the basis  $\{|\Phi_B\rangle, |01\rangle, |10\rangle, |\Phi\rangle\}$ , or

$$H_m = \sqrt{2}\Omega |00\rangle \langle \Psi_B| - \sqrt{2}\Omega e^{-i\phi} |\Psi_B\rangle \langle 11| + \text{H.c.} \quad (5)$$

in the basis  $\{|00\rangle, |\Psi_B\rangle, |\Psi\rangle, |11\rangle\}$ . Here,  $|\Phi_B\rangle = [\exp(-i\phi)|00\rangle - |11\rangle]/\sqrt{2}$  and  $|\Psi_B\rangle = [\exp(i\phi)|01\rangle - |10\rangle]/\sqrt{2}$  are orthogonal to  $|\Phi\rangle$  and  $|\Psi\rangle$ . One can see that the microwave pulses facilitate the transitions  $|01\rangle \leftrightarrow |\Phi_B\rangle \leftrightarrow |10\rangle$  and  $|00\rangle \leftrightarrow |\Psi_B\rangle \leftrightarrow |11\rangle$  within the ground-state space while leaving the states  $|\Phi\rangle$  and  $|\Psi\rangle$  as two dark states.

Based on the above ion-microwave interaction, we then introduce bichromatic lasers to facilitate transitions between ground states and excited states. The combined unitary dynamics determined by the microwave pulses and bichromatic lasers will turn one of the two dark states into a bright state while leaving another dark state as a unique dark state. By further combining the unitary dynamics with spontaneous emission, an arbitrary quantum state in ground-state space can finally be driven into one of the generalized Bell states. This is the basic idea of our scheme.

We first demonstrate the preparation of  $|\Phi\rangle$ . To this end, we introduce bichromatic lasers to drive the transitions between ground states and excited states, which turn the state  $|\Psi\rangle$  into a bright state and leave the state  $|\Phi\rangle$  as a unique dark state. The schematic setup is shown in Fig. 1. Specifically, we use a pair of blue and red sideband lasers with detunings  $-(\nu + \delta)$  and  $\nu - \delta$ , respectively, to drive the transitions  $|0\rangle \leftrightarrow |e_0\rangle$  and  $|1\rangle \leftrightarrow |e_1\rangle$  of ion 1, where  $\nu$  is the vibrational mode frequency and  $\delta$  is an additional detuning satisfying  $\delta \ll \nu$ . Meanwhile, we use another pair of blue and red sideband lasers with detunings  $-(\nu - \delta)$  and  $\nu + \delta$ , respectively, to drive the transitions  $|0\rangle \leftrightarrow |e_0\rangle$  and  $|1\rangle \leftrightarrow |e_1\rangle$  of ion 2. All the lasers share a common Rabi frequency  $\tilde{\Omega}$ . In the rotating frame and with the rotating-wave approximation, the Hamiltonian describing ion-laser interaction in the Lamb-Dicke regime reads

$$H_l = i\eta\tilde{\Omega} (a^\dagger e^{-i\delta t} |e_0\rangle_{11} \langle 0| + a e^{i\delta t} |e_1\rangle_{22} \langle 1|) + i\eta\tilde{\Omega} (a e^{-i\delta t} |e_1\rangle_{11} \langle 1| + a^\dagger e^{i\delta t} |e_0\rangle_{22} \langle 0|) + \text{H.c.}, \quad (6)$$

where  $a$  and  $a^\dagger$  are the annihilation and creation operators of the vibrational mode and  $\eta$  is the Lamb-Dicke parameter that satisfies  $\eta^2(n+1) \ll 1$ , with  $n$  being the quantum number of the vibrational mode.

If the large-detuning condition  $\delta \gg \eta\tilde{\Omega}$  is satisfied, the single-ion transitions  $|0\rangle \leftrightarrow |e_0\rangle$  and  $|1\rangle \leftrightarrow |e_1\rangle$  can be strongly suppressed while the double-ion transitions  $|01\rangle \leftrightarrow |e_0e_1\rangle$  and  $|10\rangle \leftrightarrow |e_1e_0\rangle$  are allowed by exchanging vibrational energy between two ions. By using the approach in Ref. [52], the Hamiltonian in Eq. (6) can be reduced to

$$\begin{aligned} \mathcal{H}_l = & \Delta [aa^\dagger (|e_1\rangle_{22} \langle e_1| - |e_1\rangle_{11} \langle e_1|) + a^\dagger a (|e_0\rangle_{22} \langle e_0| \\ & - |e_0\rangle_{11} \langle e_0|) + aa^\dagger (|0\rangle_{11} \langle 0| - |0\rangle_{22} \langle 0|) \\ & + a^\dagger a (|1\rangle_{11} \langle 1| - |1\rangle_{22} \langle 1|)] + (\Omega_{01} |e_0e_1\rangle \langle 01| \\ & + \Omega_{10} |e_1e_0\rangle \langle 10| + \text{H.c.}), \end{aligned} \quad (7)$$

where  $\Delta = -\Omega_{01} = \Omega_{10} = \eta^2 |\tilde{\Omega}|^2 / \delta$ . The first and second lines of the above equation are Stark shifts of excited states and ground states, respectively. The last line is the double-ion couplings between ground states and excited states. In the double-ion-state representation, the Stark shifts of the excited states can be rewritten as  $\Delta (|e_0e_1\rangle \langle e_0e_1| - |e_1e_0\rangle \langle e_1e_0|)$  and the Stark shifts of the ground states can be rewritten as  $\Delta (|01\rangle \langle 01| - |10\rangle \langle 10|)$ , where we neglect the other double-ion-state Stark shifts because they neither belong to the ground-state space nor couple with the ground-state space. To make this point clear, we give a simple derivation for the Stark shifts in the first line as  $\Delta [(|e_0\rangle \langle e_0| + |e_1\rangle \langle e_1|) \otimes (a^\dagger a |e_0\rangle \langle e_0| + aa^\dagger |e_1\rangle \langle e_1|) - (a^\dagger a |e_0\rangle \langle e_0| + aa^\dagger |e_1\rangle \langle e_1|) \otimes (|e_0\rangle \langle e_0| + |e_1\rangle \langle e_1|)] = \Delta [(aa^\dagger - a^\dagger a) |e_0e_1\rangle \langle e_0e_1| - (aa^\dagger - a^\dagger a) |e_1e_0\rangle \langle e_1e_0|] = \Delta (|e_0e_1\rangle \langle e_0e_1| - |e_1e_0\rangle \langle e_1e_0|)$  and for the Stark shifts in the second line as  $\Delta [(aa^\dagger |0\rangle \langle 0| + a^\dagger a |1\rangle \langle 1|) \otimes (|0\rangle \langle 0| + |1\rangle \langle 1|) - (|0\rangle \langle 0| + |1\rangle \langle 1|) \otimes (aa^\dagger |0\rangle \langle 0| + a^\dagger a |1\rangle \langle 1|)] = \Delta [(aa^\dagger - a^\dagger a) |01\rangle \langle 01| - (aa^\dagger - a^\dagger a) |10\rangle \langle 10|] = \Delta (|01\rangle \langle 01| - |10\rangle \langle 10|)$ . Accordingly, Eq. (7) can be rewritten as

$$\begin{aligned} \mathcal{H}_l = & \Delta (|e_0e_1\rangle \langle e_0e_1| + |01\rangle \langle 01|) \\ & - \Delta (|e_1e_0\rangle \langle e_1e_0| + |10\rangle \langle 10|) \\ & + (\Omega_{01} |e_0e_1\rangle \langle 01| + \Omega_{10} |e_1e_0\rangle \langle 10| + \text{H.c.}). \end{aligned} \quad (8)$$

From the above equation, we can readily see that under the large-detuning condition  $\delta \gg \eta\tilde{\Omega}$ , the vibrational degree of freedom is completely decoupled from the internal degree of freedom for both two-ion coupling terms and Stark-shift terms. Therefore, the unitary dynamics for the internal degree of freedom of trapped ions is independent of the vibrational quantum numbers. This implies that the collective vibrational mode does not need to be cooled to its ground state and thus the preparation works for thermally excited states.

Combining Eqs. (4) with (8), one can see that the unitary dynamics facilitate the transitions  $|01\rangle \leftrightarrow |\Phi_B\rangle \leftrightarrow |10\rangle$  within the ground-state space and the transitions  $|01\rangle \leftrightarrow |e_0e_1\rangle$  as well as  $|10\rangle \leftrightarrow |e_1e_0\rangle$  between the ground-state space and the excited-state space and leave the state  $|\Phi\rangle$  as a unique dark state. By considering the spontaneous emission from excited states  $\{|e_0\rangle, |e_1\rangle\}$  to ground states  $\{|0\rangle, |1\rangle\}$ , we can further see that a state initially prepared in  $|\Phi\rangle$  remains in  $|\Phi\rangle$ , while a state initially prepared in the other states of the ground-state space is directly or indirectly pumped to the excited-state subspace spanned by  $\{|e_0e_1\rangle, |e_1e_0\rangle\}$  via unitary dynamics and then decays to the ground-state space via spontaneous emission. The state that decays to the ground-state space is to be repumped and to redecay until it turns into the unique steady state  $|\Phi\rangle$ , as shown in Fig. 1(b). Consequently, the generalized Bell state  $|\Phi\rangle$  is prepared by combining unitary dynamics with spontaneous emission.

By using a process similar to the preparation of  $|\Phi\rangle$ , we can prepare  $|\Psi\rangle$  in Eq. (1). In fact,  $|\Psi\rangle$  can be obtained from  $|\Phi\rangle$  by swapping the states  $|0\rangle$  ( $|1\rangle$ ) for  $|1\rangle$  ( $|0\rangle$ ) of the second qubit and changing the phase  $\phi$  to  $-\phi$ .

### III. NUMERICAL SIMULATIONS

We have shown how to prepare the generalized Bell states by combining unitary dynamics with spontaneous emission. We now demonstrate the performance of our scheme with the aid of numerical simulations. To this end, we consider the instance  $|\Phi\rangle$  with  $\phi = 0$ .

First, we demonstrate the performance of our scheme under the large-detuning approximation. The unitary dynamics of our scheme are based on the Hamiltonians in Eqs. (4) and (8), where Eq. (8) is derived from the Hamiltonian in Eq. (6) under the large-detuning condition  $\delta \gg \eta\tilde{\Omega}$ . Therefore, the large-detuning approximation may affect the performance of our scheme. For our purpose, we use the fidelity

$$F = \langle \Phi | \rho(\tau) | \Phi \rangle \quad (9)$$

to characterize the performance of our scheme. This describes the closeness between  $|\Phi\rangle$  and  $\rho(\tau)$ . The state  $|\Phi\rangle$  is the target state defined in Eq. (1) and  $\rho(\tau)$  is the output state, which is obtained from the state  $\varrho(\tau)$  by tracing out the vibrational degrees of freedom. Here,  $\varrho(\tau)$  is calculated by solving the Lindblad equation [53,54]

$$\begin{aligned} \dot{\varrho}(t) = & -i[H_m + H_l, \varrho(t)] \\ & + \sum_{k=1,2} \left[ L_k \varrho(t) L_k^\dagger - \frac{1}{2} \{ L_k^\dagger L_k, \varrho(t) \} \right], \quad (10) \end{aligned}$$

where  $L_k = \sqrt{\gamma/2}|0\rangle_k \langle e_0| + \sqrt{\gamma/2}|1\rangle_k \langle e_0| + \sqrt{\gamma/2}|0\rangle_k \langle e_1| + \sqrt{\gamma/2}|1\rangle_k \langle e_1|$  is the Lindblad operator, with  $\gamma/2$

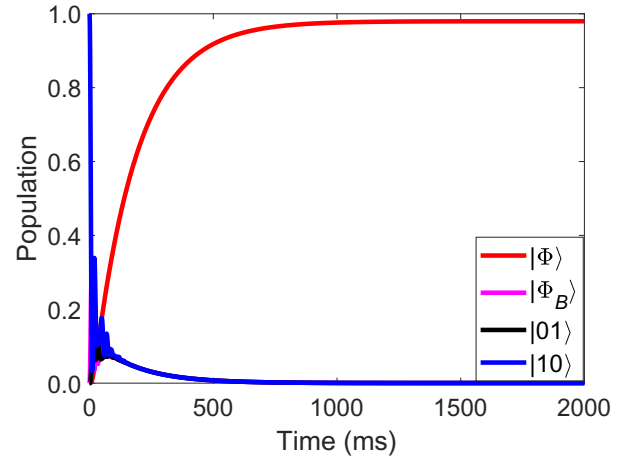


FIG. 2. The population of the basis vectors in the ground-state space. Here, we take the initial state as  $|10\rangle$ , the vibrational state as  $|0\rangle$ , and the parameters as  $\eta = 0.1$ ,  $\Omega/2\pi = 0.075$  kHz,  $\tilde{\Omega}/2\pi = 25$  kHz,  $\delta/2\pi = 50$  kHz, and  $\gamma/2\pi = 0.05$  kHz.

being the spontaneous emission rate. Therefore, the fidelity is obtained from  $\varrho(\tau)$  by first tracing out the vibrational state and then taking the overlap with the state  $|\Phi\rangle$  in Eq. (1). To complete our demonstration, we take the initial state as  $|10\rangle$ , the vibrational state (i.e., the eigenstate  $|n\rangle$  of the number operator  $a^\dagger a$ ,  $a^\dagger a|n\rangle = n|n\rangle$ ) as  $|0\rangle$ , and the parameters as  $\eta = 0.1$ ,  $\Omega/2\pi = 0.075$  kHz,  $\tilde{\Omega}/2\pi = 25$  kHz,  $\delta/2\pi = 50$  kHz, and  $\gamma/2\pi = 0.05$  kHz. It is worth noting here that we choose  $\delta = 20\eta\tilde{\Omega}$  to satisfy the large-detuning condition  $\delta \gg \eta\tilde{\Omega}$ . In Fig. 2, we plot the population  $P(t) = \langle \Phi | \rho(t) | \Phi \rangle$  as a function of the time  $t$ . The result shows the fidelity  $F = P(\tau) = 97.98\%$ , with  $\tau$  being the final time. Here, we use the population to describe the percentage of the target state in the intermediate state and we use the fidelity to describe the percentage of the target state in the output state. Thus, the fidelity is equal to the population at the final time. To visualize the dynamical process, we further plot the population  $P(t) = \langle \phi | \rho(t) | \phi \rangle$  of the other basis vectors  $|\phi\rangle \in \{|\Phi_B\rangle, |01\rangle, |10\rangle\}$  in the ground-state space. The result shows that there exists a superposition of the basis vectors at the intermediate time but there is no population of these basis vectors except for the steady state at the final time. This implies that the cooperation between unitary dynamics and spontaneous emission drives the quantum system into whole space and finally into the steady state  $|\Phi\rangle$ .

Second, we demonstrate the performance of our scheme without considering the large-detuning approximation. Above, we have obtained the fidelity of the steady state as 97.98% under the large-detuning approximation. Then, a naturally arising question is whether the limitation of the fidelity is mainly caused by the large-detuning approximation. To answer this question, we calculate the population  $P(t)$  of  $|\Phi\rangle$  by replacing the Hamiltonian  $H_l$  in Eq. (10)

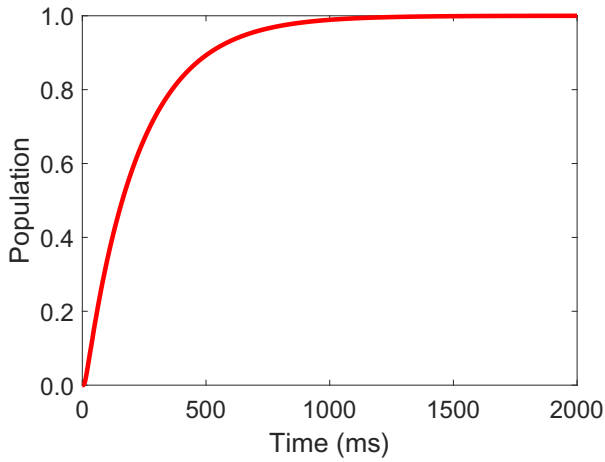


FIG. 3. The population of  $|\Phi\rangle$  without considering the large-detuning approximation. Here, we take the initial state as  $|10\rangle$ , the vibrational state as  $|0\rangle$ , and the parameters as  $\eta = 0.1$ ,  $\Omega/2\pi = 0.075$  kHz,  $\tilde{\Omega}/2\pi = 25$  kHz,  $\delta/2\pi = 50$  kHz, and  $\gamma/2\pi = 0.05$  kHz.

with the effective Hamiltonians  $\mathcal{H}_l$  in Eq. (7), which means that we do not consider the effect of the large-detuning approximation. The result is shown in Fig. 3. Here, we also take the initial state as  $|10\rangle$ , the vibrational state as  $|0\rangle$ , and the parameters as  $\eta = 0.1$ ,  $\Omega/2\pi = 0.075$  kHz,  $\tilde{\Omega}/2\pi = 25$  kHz,  $\delta/2\pi = 50$  kHz, and  $\gamma/2\pi = 0.05$  kHz. From this result, we can obtain the fidelity as  $F = P(\tau) = 99.99\%$ . This means that the final state is almost the target state  $|\Phi\rangle$  and thus the limitation of the fidelity is mainly caused by the large-detuning approximation. This result in turn indicates that the spontaneous emission does not reduce the fidelity for the chosen parameters and therefore our scheme protects entanglement from spontaneous emission.

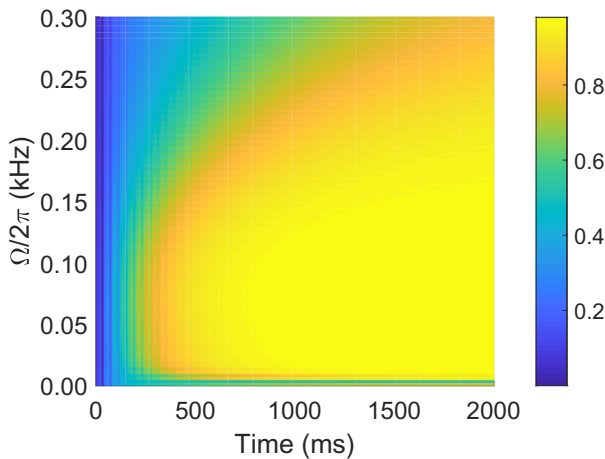


FIG. 4. The population  $P(t, \Omega) = \langle \Phi | \rho(t, \Omega) | \Phi \rangle$  as a function of  $t$  and  $\Omega$ . Here, we take the initial state as  $|10\rangle$ , the vibrational state as  $|0\rangle$ , and the parameters as  $\eta = 0.1$ ,  $\tilde{\Omega}/2\pi = 25$  kHz,  $\delta/2\pi = 50$  kHz, and  $\gamma/2\pi = 0.05$  kHz.

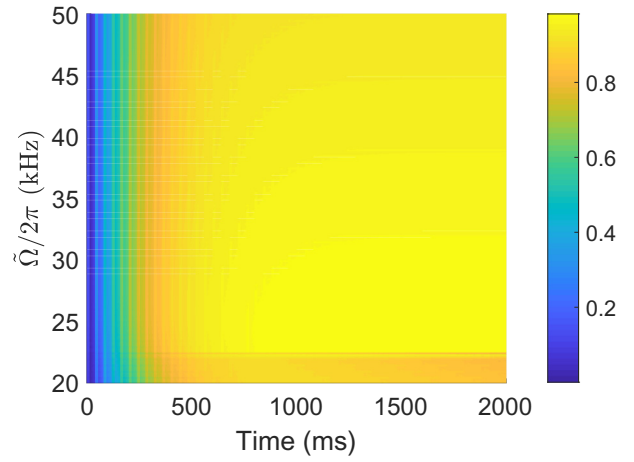


FIG. 5. The population  $P(t, \tilde{\Omega}) = \langle \Phi | \rho(t, \tilde{\Omega}) | \Phi \rangle$  as a function of  $t$  and  $\tilde{\Omega}$ . Here, we take the initial state as  $|10\rangle$ , the vibrational state as  $|0\rangle$ , and the parameters as  $\eta = 0.1$ ,  $\Omega/2\pi = 0.075$  kHz,  $\delta/2\pi = 50$  kHz, and  $\gamma/2\pi = 0.05$  kHz.

Third, we investigate the parameter ranges of microwave pulses and bichromatic lasers and the spontaneous emission rate at which we can achieve satisfactory performance. The above discussion shows that the steady state  $|\Phi\rangle$  can be obtained with a fidelity of 97.98% when  $\eta = 0.1$ ,  $\Omega/2\pi = 0.075$  kHz,  $\tilde{\Omega}/2\pi = 25$  kHz,  $\delta/2\pi = 50$  kHz, and  $\gamma/2\pi = 0.05$  kHz. We may wonder whether satisfactory performance can be also achieved when  $\Omega$ ,  $\tilde{\Omega}$  and  $\gamma$  are taken as other values. To address this, we calculate the population  $P(t, \Omega) = \langle \Phi | \rho(t, \Omega) | \Phi \rangle$  as a function of  $t$  and  $\Omega$ ,  $P(t, \tilde{\Omega}) = \langle \Phi | \rho(t, \tilde{\Omega}) | \Phi \rangle$  as a function of  $t$ , and  $\tilde{\Omega}$ , and  $P(t, \gamma) = \langle \Phi | \rho(t, \gamma) | \Phi \rangle$  as a function of  $t$  and  $\gamma$ . Here, the initial state, the vibrational state, and the two parameters  $\eta$  and  $\delta$  are taken to be the same

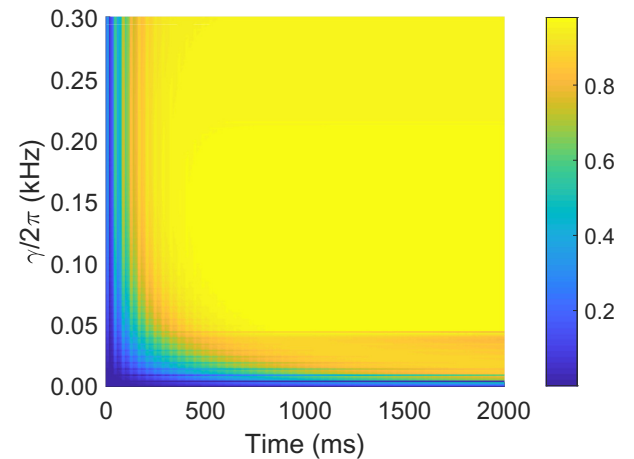


FIG. 6. The population  $P(t, \gamma) = \langle \Phi | \rho(t, \gamma) | \Phi \rangle$  as a function of  $t$  and  $\gamma$ . Here, we take the initial state as  $|10\rangle$ , the vibrational state as  $|0\rangle$ , and the parameters as  $\eta = 0.1$ ,  $\Omega/2\pi = 0.075$  kHz,  $\tilde{\Omega}/2\pi = 25$  kHz, and  $\delta/2\pi = 50$  kHz.

TABLE I. Some of the numerical data for the array  $[t, \Omega, P(t, \Omega)]$ .

$\Omega/2\pi$ (kHz)	0.005	0.01	0.045	0.065	0.07
$t = 2000$ ms	93.14%	97.10%	97.91%	97.97%	97.98%
$\tilde{\Omega}/2\pi$ (kHz)	0.075	0.08	0.095	0.15	0.19
$t = 2000$ ms	97.98%	97.97%	97.91%	97.05%	95.21%

as the previous ones, while the other three parameters,  $\Omega$ ,  $\tilde{\Omega}$ , and  $\gamma$ , are varied one at a time. That is, we take  $\tilde{\Omega}/2\pi = 25$  kHz and  $\gamma/2\pi = 0.05$  kHz when calculating  $P(t, \Omega)$ ,  $\Omega/2\pi = 0.075$  kHz and  $\gamma/2\pi = 0.05$  kHz when calculating  $P(t, \tilde{\Omega})$ , and  $\Omega/2\pi = 0.075$  kHz and  $\tilde{\Omega}/2\pi = 25$  kHz when calculating  $P(t, \gamma)$ . The results are shown in Figs. 4, 5, and 6. To clearly evaluate the performance, we present some of the numerical data for the arrays  $[t, \Omega, P(t, \Omega)]$ ,  $[t, \tilde{\Omega}, P(t, \tilde{\Omega})]$ , and  $[t, \gamma, P(t, \gamma)]$  in Tables I, II, and III, respectively. From these results, we make the following observations. (i) A wide range of intervals is allowed to achieve the steady state  $|\Phi\rangle$  with a high fidelity. For example, if  $\Omega/2\pi \in [0.01 \text{ kHz}, 0.19 \text{ kHz}]$ , the fidelity  $F = P(\tau, \Omega)$  can always be in excess of 95%; if  $\tilde{\Omega}/2\pi \in [22.5 \text{ kHz}, 39.5 \text{ kHz}]$ , the fidelity  $F = P(\tau, \tilde{\Omega})$  can always be in excess of 95%; and if  $\gamma/2\pi \in [0.045 \text{ kHz}, 0.295 \text{ kHz}]$ , the fidelity  $F = P(\tau, \gamma)$  can always be in excess of 95%. (ii) Our scheme is insensitive to fluctuations of  $\Omega$ ,  $\tilde{\Omega}$ , and  $\gamma$ . Indeed, if  $\Omega/2\pi$  ranges from 0.01 kHz to 0.15 kHz, the fidelity only varies from 97.98% to 97.05%; if  $\tilde{\Omega}/2\pi$  ranges from 22.5 kHz to 30.5 kHz, the fidelity only varies from 98.27% to 97.04%; and if  $\gamma/2\pi$  ranges from 0.045 kHz to 0.17 kHz, the fidelity only varies from 97.99% to 97.02%.

Fourth, we investigate how to match up the parameters  $\Omega$  and  $\gamma$  with a given  $\tilde{\Omega}$  in order to achieve an optimized fidelity. For this, the initial state, the vibrational state, the parameters  $\eta$  and  $\delta$ , and the final time are taken to be the same as in the above discussions. We consider three values of  $\tilde{\Omega}/2\pi$  as 20 kHz, 25 kHz, and 40 kHz in succession, which correspond to the large-detuning conditions  $\delta = 25\eta\tilde{\Omega}$ ,  $20\eta\tilde{\Omega}$ , and  $12.5\eta\tilde{\Omega}$ , respectively. With these settings, we calculate the fidelity  $F(\Omega, \gamma) = \langle \Phi | \rho(\Omega, \gamma) | \Phi \rangle$  as a function of  $\Omega$  and  $\gamma$ . The results are shown in Figs. 7, 8, and 9. Our calculations indicate that the optimized fidelities corresponding to the three given values of  $\tilde{\Omega}/2\pi$  are 98.50%, 97.99%, and

TABLE II. Some of the numerical data for the array  $[t, \tilde{\Omega}, P(t, \tilde{\Omega})]$ .

$\tilde{\Omega}/2\pi$ (kHz)	22.5	23	24	24.5	25
$t = 2000$ ms	98.27%	98.22%	98.11%	98.04%	97.98%
$\tilde{\Omega}/2\pi$ (kHz)	30.5	31	35	35.5	39.5
$t = 2000$ ms	97.04%	96.94%	96.10%	95.98%	95.04%

TABLE III. Some of the numerical data for the array  $[t, \gamma, P(t, \gamma)]$ .

$\gamma/2\pi$ (kHz)	0.045	0.065	0.07	0.085	0.17
$t = 2000$ ms	97.99%	97.91%	97.88%	97.80%	97.02%
$\gamma/2\pi$ (kHz)	0.175	0.24	0.245	0.295	0.3
$t = 2000$ ms	96.96%	96.05%	95.97%	95.09%	94.99%

95.19% and are achieved at the values  $[\tilde{\Omega}/2\pi, \Omega/2\pi, \gamma/2\pi] = [20 \text{ kHz}, 0.05 \text{ kHz}, 0.065 \text{ kHz}]$ ,  $[25 \text{ kHz}, 0.075 \text{ kHz}, 0.045 \text{ kHz}]$ , and  $[40 \text{ kHz}, 0.18 \text{ kHz}, 0.04 \text{ kHz}]$ , respectively.

Fifth, we show that our scheme works for thermally excited states. From Eq. (6), we can see that the internal degree of freedom is coupled to the vibrational degrees of freedom. Yet, under the large-detuning condition  $\delta \gg \eta\tilde{\Omega}$ , Eq. (6) is reduced to Eq. (7), which can be rewritten as Eq. (8). From Eq. (8), we can see that the vibrational degrees of freedom are completely decoupled from the internal degree of freedom for both the two-ion coupling terms and the Stark-shift terms. The merit of this decoupling is that under the large-detuning approximation, the collective vibrational mode is not necessarily cooled to its ground state and thus our scheme works for thermally excited states. Here, we should note that the above merits are valid under the large-detuning approximation. This is because Eq. (6) can only be reduced to Eq. (8) if the large-detuning condition  $\delta \gg \eta\tilde{\Omega}$  is satisfied. Considering that the large-detuning approximation promises to hold the terms in the order of magnitude  $\eta^2|\tilde{\Omega}|^2/\delta$  but to ignore the terms in the higher order of magnitude, the terms in the higher order of magnitude still strongly depend on the collective vibrational mode and thus affect the fidelity of the quantum states. To illustrate the above points, we

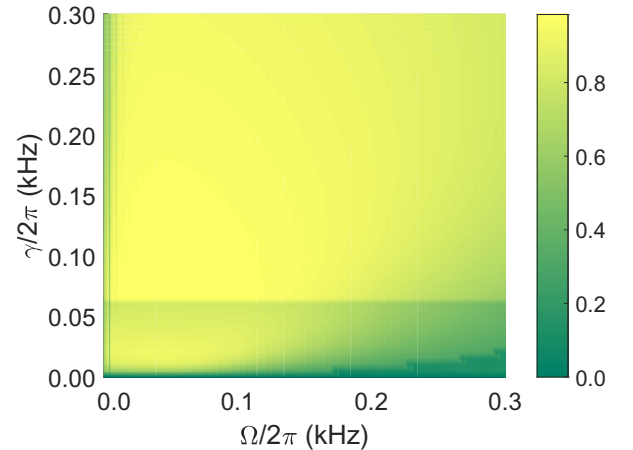


FIG. 7. The fidelity  $F(\Omega, \gamma) = \langle \Phi | \rho(\Omega, \gamma) | \Phi \rangle$  as a function of  $\Omega$  and  $\gamma$ . Here, we take the initial state as  $|10\rangle$ , the vibrational state as  $|0\rangle$ , the parameters as  $\eta = 0.1$ ,  $\tilde{\Omega}/2\pi = 20$  kHz, and  $\delta/2\pi = 50$  kHz, and the final time as 2000 ms.

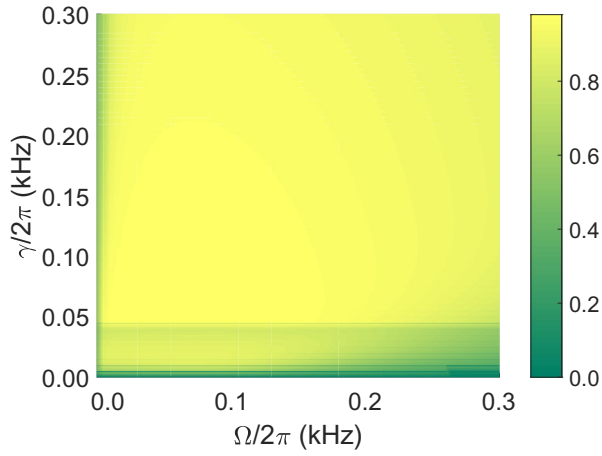


FIG. 8. The fidelity  $F(\Omega, \gamma) = \langle \Phi | \rho(\Omega, \gamma) | \Phi \rangle$  as a function of  $\Omega$  and  $\gamma$ . Here, we take the initial state as  $|10\rangle$ , the vibrational state as  $|0\rangle$ , the parameters as  $\eta = 0.1$ ,  $\tilde{\Omega}/2\pi = 25$  kHz, and  $\delta/2\pi = 50$  kHz, and the final time as 2000 ms.

plot the population  $P(t) = \langle \Phi | \rho(t) | \Phi \rangle$  as a function of  $t$  in Fig. 10. Here, we take the initial state as  $|10\rangle$ , the vibrational state as  $|n\rangle$  with  $n = 0, 1, 2$ , and the parameters as  $\eta = 0.1$ ,  $\Omega/2\pi = 0.075$  kHz,  $\tilde{\Omega}/2\pi = 25$  kHz,  $\delta/2\pi = 50$  kHz, and  $\gamma/2\pi = 0.05$  kHz. The result shows the fidelities  $F = P(\tau)$  corresponding to the vibrational states  $|0\rangle$ ,  $|1\rangle$ , and  $|2\rangle$  as being up to 97.98%, 95.22%, and 92.56%, respectively. This implies that our scheme works for thermally excited states.

In the above numerical simulations, we assume that all the decays from excited states  $\{|e_0\rangle, |e_1\rangle\}$  to ground states  $\{|0\rangle, |1\rangle\}$  have the same spontaneous emission rates. We now discuss the performance of our scheme when different decays have different spontaneous emission rates. For this,

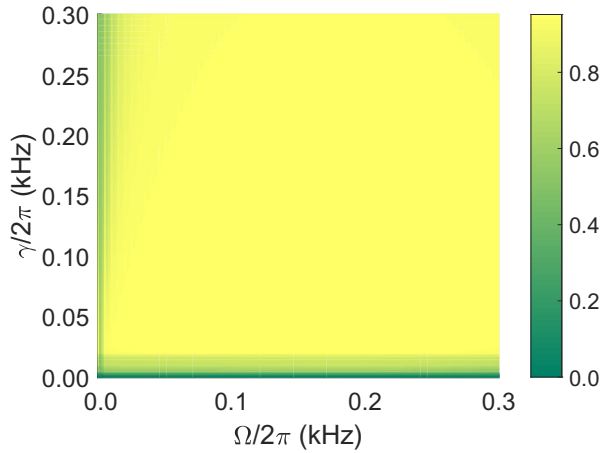


FIG. 9. The fidelity  $F(\Omega, \gamma) = \langle \Phi | \rho(\Omega, \gamma) | \Phi \rangle$  as a function of  $\Omega$  and  $\gamma$ . Here, we take the initial state as  $|10\rangle$ , the vibrational state as  $|0\rangle$ , the parameters as  $\eta = 0.1$ ,  $\tilde{\Omega}/2\pi = 40$  kHz, and  $\delta/2\pi = 50$  kHz, and the final time as 2000 ms.

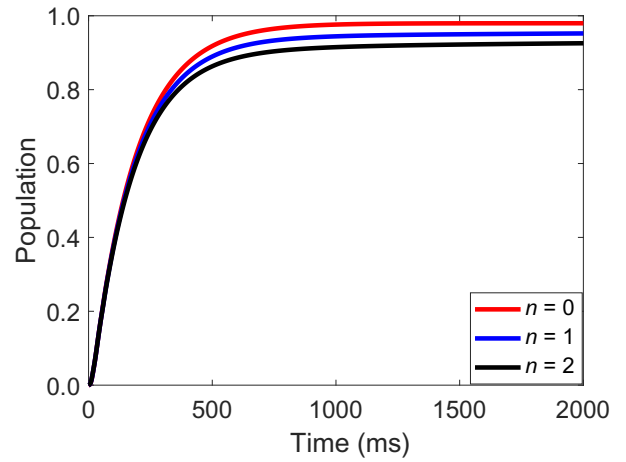


FIG. 10. The population as a function of  $t$ . Here, we take the initial state as  $|10\rangle$ , the vibrational state as  $|n\rangle$  with  $n = 0, 1, 2$ , and the parameters as  $\eta = 0.1$ ,  $\Omega/2\pi = 0.075$  kHz,  $\tilde{\Omega}/2\pi = 25$  kHz,  $\delta/2\pi = 50$  kHz, and  $\gamma/2\pi = 0.05$  kHz.

we plot the population  $P(t) = \langle \Phi | \rho(t) | \Phi \rangle$  as a function of  $t$  in Fig. 11. Here, we take the initial state as  $|10\rangle$ , the vibrational state as  $|0\rangle$ , and the parameters as  $\eta = 0.1$ ,  $\Omega/2\pi = 0.075$  kHz,  $\tilde{\Omega}/2\pi = 25$  kHz, and  $\delta/2\pi = 50$  kHz. Meanwhile, we take the Lindblad operators for different decays of ion 1 as  $L^1 = \sqrt{\gamma_1/2}|0\rangle_{11}\langle e_0|$ ,  $L^2 = \sqrt{\gamma_2/2}|1\rangle_{11}\langle e_0|$ ,  $L^3 = \sqrt{\gamma_3/2}|0\rangle_{11}\langle e_1|$ , and  $L^4 = \sqrt{\gamma_4/2}|1\rangle_{11}\langle e_1|$ , and the

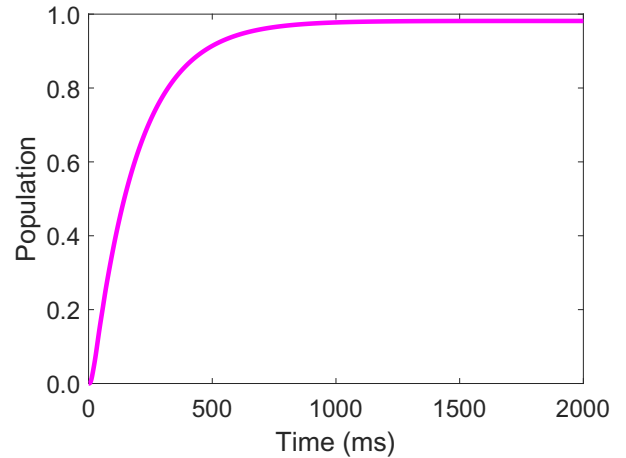


FIG. 11. The population as a function of  $t$ . Here, we take the initial state as  $|10\rangle$ , the vibrational state as  $|0\rangle$ , and the parameters as  $\eta = 0.1$ ,  $\Omega/2\pi = 0.075$  kHz,  $\tilde{\Omega}/2\pi = 25$  kHz, and  $\delta/2\pi = 50$  kHz. Meanwhile, we take the Lindblad operators for different decays as  $L^1 = \sqrt{\gamma_1/2}|0\rangle_{11}\langle e_0|$ ,  $L^2 = \sqrt{\gamma_2/2}|1\rangle_{11}\langle e_0|$ ,  $L^3 = \sqrt{\gamma_3/2}|0\rangle_{11}\langle e_1|$ ,  $L^4 = \sqrt{\gamma_4/2}|1\rangle_{11}\langle e_1|$ ,  $L^5 = \sqrt{\gamma_5/2}|0\rangle_{22}\langle e_0|$ ,  $L^6 = \sqrt{\gamma_6/2}|1\rangle_{22}\langle e_0|$ ,  $L^7 = \sqrt{\gamma_7/2}|0\rangle_{22}\langle e_1|$ , and  $L^8 = \sqrt{\gamma_8/2}|1\rangle_{22}\langle e_1|$ , with  $\gamma_1/2\pi = 0.05$  kHz,  $\gamma_2/2\pi = 0.04$  kHz,  $\gamma_3/2\pi = 0.055$  kHz,  $\gamma_4/2\pi = 0.045$  kHz,  $\gamma_5/2\pi = 0.06$  kHz,  $\gamma_6/2\pi = 0.03$  kHz,  $\gamma_7/2\pi = 0.065$  kHz, and  $\gamma_8/2\pi = 0.035$  kHz.

Lindblad operators for different decays of ion 2 as  $L^5 = \sqrt{\gamma_5/2}|0\rangle_{22}\langle e_0|$ ,  $L^6 = \sqrt{\gamma_6/2}|1\rangle_{22}\langle e_0|$ ,  $L^7 = \sqrt{\gamma_7/2}|0\rangle_{22}\langle e_1|$ , and  $L^8 = \sqrt{\gamma_8/2}|1\rangle_{22}\langle e_1|$ , with  $\gamma_1/2\pi = 0.05$  kHz,  $\gamma_2/2\pi = 0.04$  kHz,  $\gamma_3/2\pi = 0.055$  kHz,  $\gamma_4/2\pi = 0.045$  kHz,  $\gamma_5/2\pi = 0.06$  kHz,  $\gamma_6/2\pi = 0.03$  kHz,  $\gamma_7/2\pi = 0.065$  kHz, and  $\gamma_8/2\pi = 0.035$  kHz. The result shows that the fidelity  $F = P(\tau) = 98.15\%$ . This is close to the fidelity 97.98% obtained above when taking the same spontaneous emission rate for different decays.

#### IV. CONCLUSIONS

In conclusion, we propose a scheme for dissipative preparation of generalized Bell states with trapped ions. By combining unitary dynamics with spontaneous emission, an arbitrary quantum state in the ground-state space is driven into a unique generalized Bell state. Different from the previous schemes with cold trapped ions [20,21,38], the collective vibrational motion in our scheme is decoupled from the unitary dynamics so that the preparation does not need to cool the collective vibrational mode to its ground state and thus it works for thermally excited states. Compared with the scheme using two vibrational modes [22], our scheme is based on the renowned Sørensen-Mølmer setting, using only a single vibrational mode, and is therefore compatible with the current experimental technology. With the aid of numerical simulation, our scheme is demonstrated to be insensitive to variations of some parameters.

#### ACKNOWLEDGMENTS

P.Z.Z. acknowledges support from the National Natural Science Foundation of China through Grant No. 12174224 and the China Postdoctoral Science Foundation through Grant No. 2019M662318. Z.J. acknowledges support from the China Postdoctoral Science Foundation through Grant No. 20200322 and Fundamental Research Funds for the Central Universities through Grant No. N2005008.

- [1] A. K. Ekert, Quantum Cryptography Based on Bell's Theorem, *Phys. Rev. Lett.* **67**, 661 (1991).
- [2] C. H. Bennett, G. Brassard, C. Crépeau, R. Jozsa, A. Peres, and W. K. Wootters, Teleporting an Unknown Quantum State via Dual Classical and Einstein-Podolsky-Rosen Channels, *Phys. Rev. Lett.* **70**, 1895 (1993).
- [3] D. Deutsch and R. Jozsa, Rapid solution of problems by quantum computation, *Proc. R. Soc. London A* **439**, 553 (1992).
- [4] M. J. Kastoryano, F. Reiter, and A. S. Sørensen, Dissipative Preparation of Entanglement in Optical Cavities, *Phys. Rev. Lett.* **106**, 090502 (2011).
- [5] J. Busch, S. De, S. S. Ivanov, B. T. Torosov, T. P. Spiller, and A. Beige, Cooling atom-cavity systems into entangled states, *Phys. Rev. A* **84**, 022316 (2011).
- [6] F. Reiter, M. J. Kastoryano, and A. S. Sørensen, Driving two atoms in an optical cavity into an entangled steady state using engineered decay, *New J. Phys.* **14**, 053022 (2012).
- [7] R. Sweke, I. Sinayskiy, and F. Petruccione, Dissipative preparation of generalized Bell states, *J. Phys. B: At. Mol. Opt. Phys.* **46**, 104004 (2013).
- [8] S. L. Su, X. Q. Shao, H. F. Wang, and S. Zhang, Scheme for entanglement generation in an atom-cavity system via dissipation, *Phys. Rev. A* **90**, 054302 (2014).
- [9] X. Q. Shao, T. Y. Zheng, C. H. Oh, and S. Zhang, Dissipative creation of three-dimensional entangled state in optical cavity via spontaneous emission, *Phys. Rev. A* **89**, 012319 (2014).
- [10] S. L. Su, X. Q. Shao, H. F. Wang, and S. Zhang, Preparation of three-dimensional entanglement for distant atoms in coupled cavities via atomic spontaneous emission and cavity decay, *Sci. Rep.* **4**, 7566 (2014).
- [11] J. Fischbach and M. Freyberger, Steady-state entanglement enhanced by a dissipative ancilla, *Phys. Rev. A* **92**, 052327 (2015).
- [12] C. Yang, D. X. Li, and X. Q. Shao, Dissipative preparation of Bell states with parallel quantum Zeno dynamics, *Sci. China: Phys., Mech. Astron.* **62**, 110312 (2019).
- [13] Y. H. Chen, W. Qin, and F. Nori, Fast and high-fidelity generation of steady-state entanglement using pulse modulation and parametric amplification, *Phys. Rev. A* **100**, 012339 (2019).
- [14] F. Reiter, D. Reeb, and A. S. Sørensen, Scalable Dissipative Preparation of Many-Body Entanglement, *Phys. Rev. Lett.* **117**, 040501 (2016).
- [15] J. Song, Y. Xia, X. D. Sun, and H. S. Song, Dissipative preparation of multibody entanglement via quantum feedback control, *Phys. Rev. A* **86**, 034303 (2012).
- [16] R. Sweke, I. Sinayskiy, and F. Petruccione, Dissipative preparation of large  $W$  states in optical cavities, *Phys. Rev. A* **87**, 042323 (2013).
- [17] X. Q. Shao, Z. H. Wang, H. D. Liu, and X. X. Yi, Dissipative preparation of a tripartite singlet state in coupled arrays of cavities via quantum feedback control, *Phys. Rev. A* **94**, 032307 (2016).
- [18] G. D. de Moraes Neto, V. F. Teizen, V. Montenegro, and E. Vernek, Steady many-body entanglements in dissipative systems, *Phys. Rev. A* **96**, 062313 (2017).
- [19] L. T. Shen, X. Y. Chen, Z. B. Yang, H. Z. Wu, and S. B. Zheng, Steady-state entanglement for distant atoms by dissipation in coupled cavities, *Phys. Rev. A* **84**, 064302 (2011).
- [20] A. Bermudez, T. Schaetz, and M. B. Plenio, Dissipation-Assisted Quantum Information Processing with Trapped Ions, *Phys. Rev. Lett.* **110**, 110502 (2013).
- [21] C. D. B. Bentley, A. R. R. Carvalho, D. Kielpinski, and J. J. Hope, Detection-Enhanced Steady State Entanglement with Ions, *Phys. Rev. Lett.* **113**, 040501 (2014).
- [22] X. Q. Shao, Engineering steady entanglement for trapped ions at finite temperature by dissipation, *Phys. Rev. A* **98**, 042310 (2018).
- [23] F. Reiter, L. Tornberg, G. Johansson, and A. S. Sørensen, Steady-state entanglement of two superconducting qubits engineered by dissipation, *Phys. Rev. A* **88**, 032317 (2013).
- [24] P. B. Li, S. Y. Gao, H. R. Li, S. L. Ma, and F. L. Li, Dissipative preparation of entangled states between two



- spatially separated nitrogen-vacancy centers, *Phys. Rev. A* **85**, 042306 (2012).
- [25] D. D. B. Rao, S. Yang, and J. Wrachtrup, Dissipative entanglement of solid-state spins in diamond, *Phys. Rev. A* **95**, 022310 (2017).
- [26] Z. Jin, S. L. Su, and S. Zhang, Preparation of a steady entangled state of two nitrogen-vacancy centers by simultaneously utilizing two dissipative factors, *Phys. Rev. A* **100**, 052332 (2019).
- [27] A. W. Carr and M. Saffman, Preparation of Entangled and Antiferromagnetic States by Dissipative Rydberg Pumping, *Phys. Rev. Lett.* **111**, 033607 (2013).
- [28] D. D. B. Rao and Klaus Mølmer, Deterministic entanglement of Rydberg ensembles by engineered dissipation, *Phys. Rev. A* **90**, 062319 (2014).
- [29] X. Q. Shao, J. B. You, T. Y. Zheng, C. H. Oh, and S. Zhang, Stationary three-dimensional entanglement via dissipative Rydberg pumping, *Phys. Rev. A* **89**, 052313 (2014).
- [30] S. L. Su, Q. Guo, H. F. Wang, and S. Zhang, Simplified scheme for entanglement preparation with Rydberg pumping via dissipation, *Phys. Rev. A* **92**, 022328 (2015).
- [31] S. L. Su, Y. Z. Tian, H. Z. Shen, H. P. Zang, E. J. Liang, and S. Zhang, Applications of the modified Rydberg antiblockade regime with simultaneous driving, *Phys. Rev. A* **96**, 042335 (2017).
- [32] X. Q. Shao, J. H. Wu, and X. X. Yi, Dissipative stabilization of quantum-feedback-based multipartite entanglement with Rydberg atoms, *Phys. Rev. A* **95**, 022317 (2017).
- [33] X. Chen, H. Xie, G. W. Lin, X. Shang, M. Y. Ye, and X. M. Lin, Dissipative generation of a steady three-atom singlet state based on Rydberg pumping, *Phys. Rev. A* **96**, 042308 (2017).
- [34] X. Chen, G. W. Lin, H. Xie, X. Shang, M. Y. Ye, and X. M. Lin, Fast creation of a three-atom singlet state with a dissipative mechanism and Rydberg blockade, *Phys. Rev. A* **98**, 042335 (2018).
- [35] Y. H. Chen, Z. C. Shi, J. Song, Y. Xia, and S. B. Zheng, Accelerated and noise-resistant generation of high-fidelity steady-state entanglement with Rydberg atoms, *Phys. Rev. A* **97**, 032328 (2018).
- [36] R. Li, D. M. Yu, S. L. Su, and J. Qian, Periodically driven facilitated high-efficiency dissipative entanglement with Rydberg atoms, *Phys. Rev. A* **101**, 042328 (2020).
- [37] Z. Jin, W. J. Gong, A. D. Zhu, S. Zhang, Y. Qi, and S. L. Su, Dissipative preparation of qutrit entanglement via periodically modulated Rydberg double antiblockade, *Opt. Express* **29**, 10117 (2021).
- [38] Y. Lin, J. P. Gaebler, F. Reiter, T. R. Tan, R. Bowler, A. S. Sørensen, D. Leibfried, and D. J. Wineland, Dissipative production of a maximally entangled steady state of two quantum bits, *Nature* **504**, 415 (2013).
- [39] S. Shankar, M. Hatridge, Z. Leghtas, K. M. Sliwa, A. Narla, U. Vool, S. M. Girvin, L. Frunzio, M. Mirrahimi, and M. H. Devoret, Autonomously stabilized entanglement between two superconducting quantum bits, *Nature* **504**, 419 (2013).
- [40] M. E. Kimchi-Schwartz, L. Martin, E. Flurin, C. Aron, M. Kulkarni, H. E. Tureci, and I. Siddiqi, Stabilizing Entanglement via Symmetry-Selective Bath Engineering in Superconducting Qubits, *Phys. Rev. Lett.* **116**, 240503 (2016).
- [41] X. Wang, H. L. Zhang, W. G. Zhang, X. L. Ouyang, X. Z. Huang, Y. F. Yu, Y. Q. Liu, X. Y. Chang, D. L. Deng, and L. M. Duan, Entangling nuclear spins by dissipation in a solid-state system, *Phys. Rev. A* **102**, 032615 (2020).
- [42] S. B. Zheng, Quantum Logic Gates for Hot Ions without a Speed Limitation, *Phys. Rev. Lett.* **90**, 217901 (2003).
- [43] A. Sørensen and K. Mølmer, Quantum Computation with Ions in Thermal Motion, *Phys. Rev. Lett.* **82**, 1971 (1999).
- [44] A. Sørensen and K. Mølmer, Entanglement and quantum computation with ions in thermal motion, *Phys. Rev. A* **62**, 022311 (2000).
- [45] L. Deslauriers, S. Olmschenk, D. Stick, W. K. Hensinger, J. Sterk, and C. Monroe, Scaling and Suppression of Anomalous Heating in Ion Traps, *Phys. Rev. Lett.* **97**, 103007 (2006).
- [46] I. Talukdar, D. J. Gorman, N. Daniilidis, P. Schindler, S. Ebadi, H. Kaufmann, T. Zhang, and H. Häffner, Implications of surface noise for the motional coherence of trapped ions, *Phys. Rev. A* **93**, 043415 (2016).
- [47] A. E. Webb, S. C. Webster, S. Collingbourne, D. Breaud, A. M. Lawrence, S. Weidt, F. Mintert, and W. K. Hensinger, Resilient Entangling Gates for Trapped Ions, *Phys. Rev. Lett.* **121**, 180501 (2018).
- [48] J. Benhelm, G. Kirchmair, C. F. Roos, and R. Blatt, Towards fault-tolerant quantum computing with trapped ions, *Nat. Phys.* **4**, 463 (2008).
- [49] T. P. Harty, M. A. Sepiol, D. T. C. Allcock, C. J. Ballance, J. E. Tarlton, and D. M. Lucas, High-Fidelity Trapped-Ion Quantum Logic Using Near-Field Microwaves, *Phys. Rev. Lett.* **117**, 140501 (2016).
- [50] T. Manovitz, A. Rotem, R. Shaniv, I. Cohen, Y. Shapira, N. Akerman, A. Retzker, and R. Ozeri, Fast Dynamical Decoupling of the Mølmer-Sørensen Entangling Gate, *Phys. Rev. Lett.* **119**, 220505 (2017).
- [51] Y. Shapira, R. Shaniv, T. Manovitz, N. Akerman, and R. Ozeri, Robust Entanglement Gates for Trapped-Ion Qubits, *Phys. Rev. Lett.* **121**, 180502 (2018).
- [52] D. F. V. James and J. Jerke, Effective Hamiltonian theory and its applications in quantum information, *Can. J. Phys.* **85**, 625 (2007).
- [53] G. Lindblad, On the generators of quantum dynamical semigroups, *Commun. Math. Phys.* **48**, 119 (1976).
- [54] V. Gorini, A. Kossakowski, and E. C. G. Sudarshan, Completely positive dynamical semigroups of  $N$ -level systems, *J. Math. Phys.* **17**, 821 (1976).